UNIVERSITY OF TURKU

Enhancing the Stability of Copper Nanowires via 2D MXene Surface Coating

Materials Chemistry, Department of Chemistry

Master's thesis

Author:
Aman Kumar

1.12.2025

Turku

Acknowledgement

I would like to extend my heartfelt gratitude and thanks to my supervisors, Prof. Carita Kvarnström and Ass. Prof. Vipul Sharma for their constructive feedback and support throughout this thesis work. I would also like to thank my supervisor and mentor Dr. Rituporn Gogoi, for the valuable advice, insightful discussions, and hands-on assistance throughout the process.

I am grateful to the Department of Mechanical and Materials Engineering, as well as the Department of Chemistry at the University of Turku, for providing an encouraging environment and the facilities necessary for completing my thesis.

I would like to express my appreciation for my colleagues and friends, Amit Barua, Kristofer Kolpakov, Ana-Marija Pitner, Timo Laukkanen, and Shaharyar Siddiqui, for their moral support and encouragement. Finally, I am thankful to my family for their belief in me and their patience during the process.

Master's thesis
Subject: Chemistry
Author: Aman Kumar
Title: Enhancing the Stability of Copper Nanowires via 2D MXene Surface Coating
Supervisors: Prof. Carita Kvarnström, Ass. Prof. Vipul Sharma, Dr. Rituporn Gogoi
Number of pages: 34 pages
Date: 1.12.2025

Abstract:

Copper nanowires (CuNWs) are a promising material for flexible, transparent electronics. CuNWs showcase mechanical flexibility and conductivity, which is comparable to that of silver nanowires, along with cost-effectiveness. However, the long-term applications of CuNWs are directly affected by oxidation, which induces surface degradation, thereby diminishing the material's environmental resistance. In this thesis, we have developed a Copper nanowire-MXene nanocomposite (Cu-MXene) via a 2-step method to enhance the lifetime of the CuNWs by protecting them from oxidation. MXenes are a class of two-dimensional (2D) transition metal carbides which exhibit outstanding electrical conductivity, hydrophilicity and chemical stability, making them an ideal candidate for CuNWs protection.

In this study, CuNWs were synthesised using a hydrothermal method using D- (+)-glucose as a reducing agent and hexadecyl amine as a capping agent to control the nanomaterial morphology and aspect ratio. The as-prepared CuNWs were incorporated with MXene ($Ti_3C_2T_X$, where X is O, OH, F, etc.) via adsorption at low temperature (<5 °C), establishing interfacial interactions between CuNWs and $Ti_3C_2T_X$. The structural, morphological and chemical properties of the Cu-MXene composite were determined using Scanning electron microscopy (SEM), Transmission electron microscopy (TEM), X-ray diffraction (XRD), and X-ray photoelectron spectroscopy (XPS). The electrical conductivity and oxidation resistance were determined using four-probe and degradation studies over time, respectively.

The electron microscopies reveal the formation of ultralong CuNWs, with a diameter of 60 ± 0.3 nm and >100 μm long. The combined characterisation results demonstrate strong interfacial interactions between MXene and CuNWs, encompassing both physical and conformal contact and electrical bridging. Degradation studies further reveal that MXene serves as an effective protective layer against oxidation.

This thesis introduces an MXene-based strategy to enhance CuNW durability and paves the way for optimised composites and device integration.

Key-words: CuNWs, MXene, $Ti_2C_2T_X$, Cu-MXene Composite nanowires

Table of contents

Abbreviations

Flexible conductive electrodes (FCEs)

Organic light-emitting diodes (OLEDs)

Indium tin oxide (ITO)

Copper nanowires (CuNWs)

Silver nanowires (AgNWs)

Gold nanowires (AuNWs)

Metal nanowires (MNWs)

Metal nanowire-based Flexible transparent conductive electrodes (MFCTEs)

Zero-dimensional (0D)

One-dimensional (1D)

Two-dimensional (2D)

Transparent conductive oxides (TCOs)

UV-Visible Spectroscopy (UV-Vis)

Fourier Transform Infrared Spectroscopy (FTIR)

X-ray Diffraction (XRD)

X-ray Photoelectron Spectroscopy (XPS)

Scanning Electron Microscopy (SEM)

Secondary electrons (SE)

Backscattered electrons (BSE)

Energy-dispersive X-ray spectroscopy (EDS)

Transmission Electron Microscopy (TEM)

High-resolution TEM (HRTEM)

Selected Area Electron Diffraction (SAED)

Electron Energy Loss Spectroscopy (EELS)

Copper-MXene composite nanowires (Cu-MXene)

Vapour-Liquid-Solid (VLS)

Chemical Vapour Deposition (CVD)

Attenuated Total Reflectance (ATR)

1. Introduction:

Flexible conductive electrodes (FCEs) have gained significant interest in the scientific and industrial communities in recent years, due to their wide range of applications. They are used extensively in various sectors, including the manufacturing of touch screens, flat displays, solar cells, organic light-emitting diodes (OLEDs), and memory devices. [1], [2] An ideal FCE is expected to showcase the following characteristics: significant optoelectronic properties, good mechanical strength and flexibility, and some resistance to corrosion in various environments, as well as ease of processing. A general FCEs architecture consists of several essential components. It includes a Flexible substrate, which provides transparency and mechanical resilience, and a conductive layer, which conducts electricity while maintaining transparency. Adhesion layers are applied to promote bonding between the conductive layer and the substrate, while protective layers prevent oxidation, moisture ingress and mechanical damage. Additionally, edge interfaces enable the electrical connection between the electrode and external circuits.[3] Conductivity is very crucial for transparent conductors, and choosing a suitable material for the conducting layer very much influences the performance of the FCTEs. Over the period of time, Zero-dimensional (0D), One-Dimensional (1D), Two-dimensional (2D) conductive polymers, transparent conductive oxides (TCOs), and hybrids (composite materials) are some of the materials which have been studied thoroughly. Currently, the widely used commercially available material for fabricating transparent electrodes is thin-film indium tin oxide (ITO). ITO possesses both low sheet resistance ($\leq$10 Ω sq^{-1}) and high optical transparency (<90 %). However, ITO films exhibit several drawbacks, for instance, the mechanical fragility of ITO films, which is a TCO, expensive and low-throughput production due to the scarcity of Indium, and high cost of high-vacuum deposition-based film manufacturing limit further use of the material in flexible electronics.[4]

Initially, as alternatives, other transparent conductive oxides, such as fluorine-doped tin oxide, aluminium-doped zinc oxide, were investigated.[5] However, The mechanical flexibility of these materials was not far from that of ITO. Further, Solution-processed transparent electrodes using carbon nanotubes, graphene, and conducting polymers were also investigated. Nevertheless, the carbon nanotubes, particularly single-walled carbon nanotube thin films, suffered from high contact resistance. Graphene-based electrodes showcased promising results, but the fabrication of defect-free single-grain graphene has high-cost production methods, and conductive polymers exhibit lower electrical conductivity, lower optical transparency, and limited tunability options.[4]

Metal-based materials, particularly metal nanowires (MNWs), including silver nanowires (AgNWs), platinum nanowires (PtNWs), copper nanowires (CuNWs), gold nanowires (AuNWs) and other nanowires with a core-shell structure. Owing to their outstanding optoelectronic properties, solution treatability, compatibility with semiconductors, and exceptional mechanical strength makes MNWs promising alternative to ITO.[6], [7] [8] Comparative studies have revealed that MNWs-based FCEs (MFCEs) exhibit better electrical conductivity and higher transmittance to ITO-based electrodes. Additionally, a higher yield strength (≤ 2.64 GPa) and a remarkable figure of merit (the relationship between light transmittance at 550 nm and sheet resistance) highlight the distinction between the two. There is a lot of room for improvement in the field of MFCTEs, as is evident by the increase in the power conversion efficiency of organic solar cells from 10% to 18% in the last few years. MNWs such as AuNWs and PtNWs are desirable alternatives to ITO, given their stability and resistance to corrosive environments. Both metals are scarce in Earth's crust, and the synthesis process for both the nanowires requires exact control and a specific environment, which limits the widespread application of these nanowires. On the other hand, CuNWs and AgNWs are the two most studied metal nanowires due to their high intrinsic electrical conductivity. However, elemental copper is roughly 700 times more abundant and 100 times cheaper than silver, with a comparative electrical conductivity to silver. The cost-effectiveness of CuNWs is the factor that makes them more desirable than AgNWs; moreover, extensive research has been done, which demonstrates high-performance FCEs based on CuNW networks. Even so, oxidation of CuNWs under ambient conditions remains a major drawback which is limiting the use of CuNW networks on a large scale.

Over the period of time, multiple studies have been developed, for instance, tailoring core shell structures, deposition of protective coating layer with metal oxides, sulfides and hydroxides, deposition of carbonaceous materials and polymers.[9], [10], [11] Fabrication of metal shell layers on top of CuNWs to obtain a core-shell structure via solution-based fabrication methods such as Cu-Ni, Cu-Ag, Cu-Au, Cu-Sn, Cu-Zn and Cu-Pt was conducted. However, CuNWs seem to degrade faster due to their inherent instability in aqueous and corrosive media. Furthermore, controlling uniform coating and thickness of the metallic shell layer is not easily achieved, which may alter the performance of the resulting FCEs.[9] Another widely adopted method is to coat CuNWs using carbonaceous material; some of the most common coatings are reduced graphene oxide, fluorene and carbon nanotubes.[10] The stability of CuNWs-based FCEs has also improved significantly by the co-encapsulation of oxidation-prone Cu and impermeable graphene.[11] However, there are several obstacles when it comes to application,

(i) nanogaps between the MNWs increase junction resistance, which limits the charge transport and reduces the performance of optoelectronic devices[12] (ii) the large surface roughness is unfavorable for the deposition of any functional layer[13] (iii) oxidation or sulfidation of MNWs occurs in ambient conditions[14] which further lowers the electric performance. This further solidifies the fact that this field is growing at an exponential rate and needs to be further scrutinised.

Another class of materials ~~exhibits~~ which exhibit distinct characteristics are 2D materials like graphene, hexagonal boron nitride (h-BN), Thin metal dichalcogenides (TMDs), e.g., Molybdenum disulfide (MoS_2), vanadium disulfide (VS_2), and newer families like MXenes are atomically thin sheets with large lateral dimensions and extremely small thickness.[1], [15]Materials like graphene offer extremely high carrier mobility and transparency (~97 % transmittance per monolayer). Additionally, TMDs provide semiconducting behaviour with sizeable band gaps for digital/optoelectronic uses. 2D layers provide continuous coverage, lowering the need for percolation networks and offering improved contact strategies. furthermore, Van-der-Waals stacking allows designers to create heterostructures without lattice matching; surfaces are accessible for functionalization (sensors, catalysis). Also, high Young's modulus and low bending stiffness allow conformity to curved substrates. Despite the potential of 2D materials, some aspects still require improvement. Atomically-thin sheets are flexible but not highly stretchable, so additional structuring is needed for truly stretchable devices. Chemical vapour deposition (CVD) films are often polycrystalline with grain boundaries that degrade mobility and uniformity for long-area electronics[16]

Composite nanowire systems combine 1D and 2D components in networked, layered or core-shell configurations to exploit complementary properties. 1D nanowires create long-range percolation while 2D sheets provide planar conduction and fill gaps, reducing junction resistance and improving uniformity.[17] This dual transport reduces the impact of individual wire-wire contacts. 2D layers can encapsulate or mechanically support 1D networks, strain, and prevent crack propagation. Therefore, networks show improved bending and stretch cycling durability.[18] 2D coatings can encapsulate oxidation-prone nanowires, protecting them from air and humidity while preserving conductivity. Charge transfer across 1D and 2D composite nanowires can enhance photocatalytic activity,[19] sensing sensitivity[20] and electrocatalysis.[21] The use of hybrids have lead to high-performance supercapacitors, FCEs, sensors and robust transparent electrodes[18]

Recent advances in two-dimensional (2D) materials have introduced a new class of surface modifiers, MXenes, which might be able to overcome these limitations.[15] MXenes are a

family of 2D materials with the general formula of composition as $M_{n+2}X_nT_x$, where M represents an early transition metal, 'X' represents carbon and/or nitrogen, and 't' represents the surface terminations such as oxygen (O), hydroxyl (-OH), fluoride (-F) and /or chloride (-Cl), with n = 1, 2, 3 and 'X' represent the number of terminal groups. This group of materials have many diverse properties, for example, High electric conductivity, significant electrochemical capacitance, good mechanical strength, thermal stability, tunable plasmonic characteristics and optical transparency.[22] Over 60 MXenes have been reported to date. Among all these various MXenes, $Ti_3C_3T_x$ has been most extensively studied due to its favourable synthesis and superior electrical characteristics.

Following ~~in~~ the same approach, this thesis demonstrates the successful synthesis of CuNWs via a simple hydrothermal process. Additionally, Copper MXene composite nanowires (Cu-MXene) were successfully formed using a simple solution-based method. Furthermore, the effect of $Ti_3C_2T_x$ MXene as a protective layer in ambient conditions is also discussed. The objective of the thesis is to provide a scalable and versatile MXene-based strategy for improving CuNW durability and showcasing the interactions between the materials.

1.1 Synthesis Strategies for 1D, 2D and Hybrid 1D/2D Nanomaterials:

Over time, multiple shape-controlled synthesis methods have been developed to create MNWs, keeping in mind the following characteristics: (i) control dimensions and morphology of the products, (ii) cost effectiveness, (iii) reproducibility, and (iv) recyclability. Additionally, 2D materials exhibit unique optical, electrical and mechanical properties, making them vital for next-generation nanotechnology. The discovery of graphene in 2004 led to a surge of interest in 2D materials such as TMDs, h-BN, bio-based graphene, and MXenes.[15][23] In this section, we will be discussing different synthesis processes such as (i) vapour phase synthesis, (ii) template-assisted synthesis and (iii) solution phase synthesis. The synthesis strategies can be broadly categorised into top-down, bottom-up and hybrid approaches **(Fig. 1)**. Each offering has distinct advantages and challenges.[7] [8] [23]

Top-down methods rely on miniaturising bulk material through advanced lithographic or etching techniques to achieve nanoscale precision, making them ideal for the fabrication of MNWs and 2D nanomaterials where structural accuracy is critical. In contrast, bottom-up methods construct nanostructures atom by atom or molecule by molecule through controlled chemical and physical growth processes, providing scalability, materials diversity, and superior crystallinity. For 2D materials, top-down methods rely on exfoliating bulk materials into thin

layers, while bottom-up techniques assemble 2D materials atom-by-atom through chemical or physical growth. Together, these approaches provide complementary pathways for the synthesis of MNWs and 2D materials, balancing precision engineering with high-quality material growth.[24]

Hybrid materials that combine 1D structures, such as nanotubes or nanowires with 2D layered sheets like graphene, MXenes, or MoS_2, have become an important direction in advanced electronics. These mixed-dimensional architectures integrate the unique advantages of both material types, axial conductivity and high aspect ratio from 1D materials, large surface area and strong in-plane transport from 2D layers. The resulting 1D/2D hybrids form interconnected, mechanically robust and highly conductive networks that overcome the limitations of each material individually.[25] .

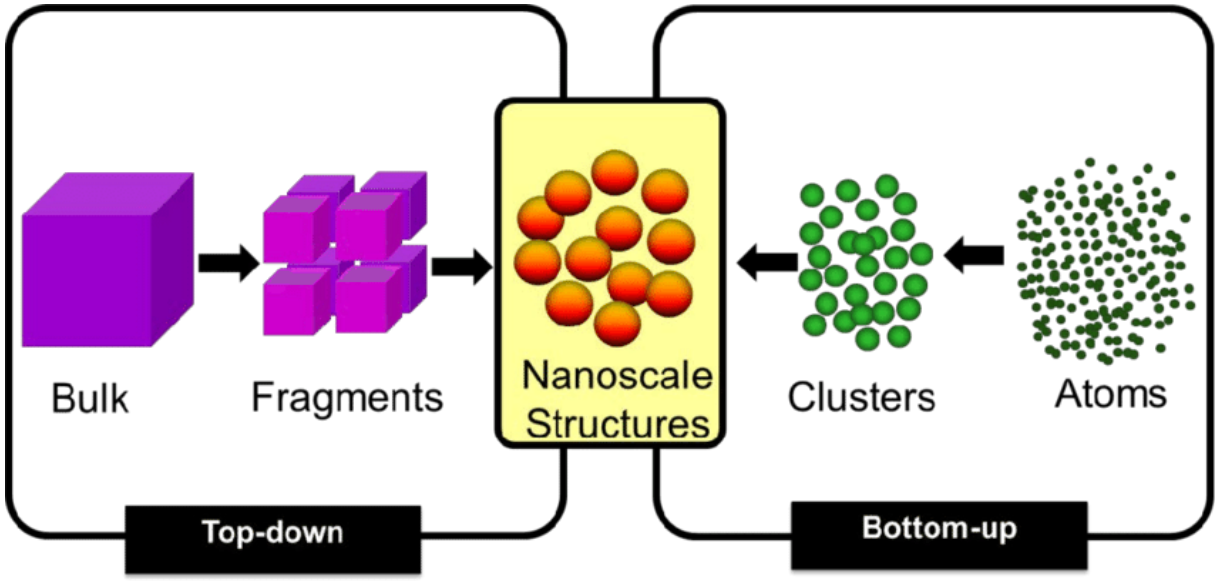

Fig. 1 Illustration of the Top-down and Bottom-up approaches for material synthesis

(a) Synthesis Strategies for 1D Nanomaterials

Top-down synthesis involves fabricating nanowires by carving, etching and patterning bulk materials into 1D structures. The approach begins with a solid substrate, and various physical and chemical processes are applied to achieve nanoscale features. these techniques provide excellent dimensional precision and alignment, making them ideal for electronics and photonic applications. However, they are expensive and often limited to small-scale production. One such strategy is Lithography-Based methods, which involves defining nanowire shapes by transferring patterns onto a substrate using light, electrons, or mechanical moulds, followed by

selective material removal. the pattern dictates the nanowires' dimensions and arrangements. Electron Beam Lithography and Nanoimprint Lithography are two variants of lithography-based techniques. Electron Beam Lithography uses a focused electron beam to write nanoscale patterns on a resist. After developing and etching, nanowires are formed with near-atomic precision. Widely used for Si and Gallium arsenide (GaAs) nanowires. Nanoimprint Lithography mechanically presses a mould onto a polymer resist to imprint nanoscale patterns. After cutting and etching, uniform nanowire arrays are produced. Compatible with flexible and large area applications.[24] Ion and Plasma-Based Etching is one such method in which materials are selectively removed from the substrate using energetic ions or chemically reactive plasma, sculpting nanowires from a bulk film, often combined with lithography for precise control. Some of the techniques which come under the umbrella of ion and plasma-based etching are Focused Ion Beam milling and reactive Ion etching. The basic principle for this method is, a highly focused ion beam physically sputters material from targeted regions, creating custom nanowire geometries without masks. Reactive ion etching uses plasma-generated reactive species to etch the material anisotropically; it is often used with lithography to produce Si and ZnO nanowire arrays.

Major advantages of Top-Down strategies are that these methods provide precise control over size, alignment and position. these methods are highly reproducible and are compatible with device fabrication. Additionally, it can be used to produce clean and ordered structures, with the only downside being high cost and low throughput and potential structural damage from ion/electron beam.[26]

Bottom-Up synthesis assembles nanowires from atoms, ions or molecules through chemical or physical growth. These methods produce highly crystalline, scalable and compositionally diverse nanostructures, with subclasses categorised based on the environment in which growth occurs. Nanowires are synthesised from gaseous precursors that nucleate and grow on catalysts or directly on substrates during Vapour-Phase synthesis. Growth is anisotropic due to preferential deposition along certain crystallographic directions. There are several different strategies in which the vapour phase technique can be utilised; some of these methods are as follows: Vapour-Liquid-Solid (VLS) Growth**.** In this method, a liquid nanoparticle catalyst absorbs vapourised precursor atoms.[27] When supersaturation occurs, the material precipitates at the solid-liquid interface, forming nanowires. Further, Vapour-Solid-Solid is Similar to VLS, but the catalyst remains solid. precursor atoms diffuse through or over the solid catalyst to the growth front. This method is usually used for compound semiconductor nanowires. Up next, Chemical Vapour Deposition (CVD)**,** during this process, precursors decompose or react on a

heated substrate to form nanowires directly, without a liquid catalyst. Enables uniform growth of Zn, SnO_2, and Si nanowires. Lastly, in Aerosol Assisted CVD, aerosolised liquid precursors are transported to the heated substrate, where they decompose to form nanowires. Allows lower temperature deposition for oxide nanowires. [28]

The process of Solution-Phase Synthesis involves growing nanowires in liquid media via controlled chemical reactions, often guided by surfactants or catalysts, promoting anisotropic growth**.** Solution-Liquid-Solution growth is one of the types of solution-phase synthesis. In this process, a liquid metal catalyst in a solvent absorbs precursors that precipitate at supersaturation, forming nanowires. This method is suitable for compound and core-shell nanowires. Next is Hydrothermal and Solvothermal Synthesis, in which reactions occur in sealed vessels at elevated temperature and pressure, driving anisotropic crystal growth. common for ZnO, TiO_2, and MnO_2 nanowires. Additionally, the Sol-Gel Process is one of the processes in which the precursors undergo hydrolysis and condensation in solution to form gels, which are converted into nanowires upon healing which provides chemical homogeneity and stoichiometric control. In the template-assisted synthesis process**,** fabrication of free-standing nanowires is achieved with the help of templates, which are designed to direct the nucleation and growth of the material nanowires. Widely, there are two accepted template types: soft (bacteria, DNA stars, rod-shaped viruses) and hard templates (porous alumina, carbon nanotubes, polymeric templates). After the formation of the nanowires, depending on the type, these templates can be removed by a simple etching or calcination method. Electrochemical deposition is one of the methods which is employed within this technique, during which metal ions are reduced within the pores of the templates, like anodised aluminium oxide, forming nanowires that match the pore geometry. Whereas, Sol-Gel or CVD infiltration is the process in which precursor materials fill the template pores via sol-gel chemistry or vapour pressure deposition. Subsequent treatment converts them into nanowires. Some of the advantages of these methods are high purity nanowires, single crystalline structure, cost-effective and scalable and good compositional control. On the other hand, it has some disadvantages, such as alignment and positioning are limited, template removal can introduce defects, and catalyst/solvent contamination is possible.[29]

Additionally, hybrid approaches integrate top-down structural control with bottom-up chemical growth, enabling aligned site-specific nanowire arrays with tunable properties. Plasma and Laser-Based Hybrid Techniques are one of the examples of composite hybrids. In this process, external energy sources like plasma or laser promote precursor decomposition or ablation, combining physical and chemical growth control. In addition, Plasma Enhanced

Chemical Vapour Deposition is one of the processes which uses plasma to activate chemical reactions at lower substrate temperatures, allowing vertically aligned nanowires. Another example of such a combination is laser ablation, in which a high-energy laser vaporises a target, forming a plume that condenses into nanowires used for carbon and silicon nanowires. Additionally, Lithography-Guided Growth is another type of composite hybrid technique. In this process, predefined catalyst positions via lithography direct bottom-up growth at specific sites, ensuring precise alignment. One such example is lithography-guided VLS, as the procedure proceeds, a catalyst pattern guides VLS growth to produce aligned arrays, such as GaN and Si nanowires, for optoelectronic devices. These processes combine structural precision with controlled growth, produce site-specific, vertically aligned nanowires, reduce contamination and improve reproducibility. Despite this, the process is a complex, multistep, with limited scalability and high cost.[30]

(b) Synthesis Strategies for 2D Nanomaterials

Mechanical exfoliation is one such process which involves peeling or tearing layers from a bulk crystal using adhesive tapes or mechanical force. The Van der Waals forces between layers are overcome by applying normal and lateral forces to isolate monolayers. Using this process can produce defect-free and pristine monolayers and is pocket-friendly. Despite this, this process requires precise handling and high-quality bulk material, and it suffers from low yield and scalability issues. MoS_2, WSe_2 and graphene are some of the materials that can be produced using this process.[31] Similarly, in liquid-phase and chemical exfoliation, the basic mechanism involves bulk layered materials being dispersed in solvents, and sonication or ion intercalation is used to separate the layers. Chemical exfoliation introduces ions or molecules between layers to weaken van der Waals bonds to form single layers or fewer layers of 2D materials. Despite being scalable and suitable for a variety of materials, this process produces smaller flakes with defects, and the solvent residue in the reaction mixture might affect the purity.[32]

Chemical vapour deposition comprises the vaporisation of precursors and reacting them at elevated temperatures to deposit thin films on substrates, resulting in thin layers of 2D materials. Using this process, uniform and long-area monolayers of tunable thickness and morphology of 2D materials can be synthesised.[33] One downside to this process is the possible formation of defects during the transfer. Furthermore, the epitaxial growth process requires the deposition of atoms or molecules on a crystalline substrate where the 2D layer aligns epitaxially with the substrate lattice. Via this process, highly oriented and crystalline films can be produced, which

are suitable for van der Waals heterostructures.[34] This process is limited by lattice mismatch, and it requires atomically smooth substrates. Some examples such as topochemical and wet-chemical growth, and bio-based and green synthesis**.** During topochemical and wet-chemical growth, the precursor transforms while retaining its structure and the process is conducted in a solution or vapour phase under controlled conditions. Synthesis of complex compounds can be enabled using this synthesis process; also, the stoichiometry and morphology of the material can be controlled. The process involves elevated temperatures and involves multiple reaction steps, creating scalability and economic issues. Bio-based and green synthesis process involves the utilisation of renewable and waste-derived carbon sources such as plant oil, lignin, food waste, etc., for the formation of carbon-based 2D materials under CVD or catalytic conditions. The process is environmentally friendly and sustainable, cost-effective and uses renewable feedstock. A multistep purification process at high temperatures has to be integrated with the main processes to ensure the quality of the material.[33]

(c) Synthesis Strategies for 1D/2D Hybrid Nanomaterials

The ability to form hierarchical architectures, super restacking and facilitate efficient charge transport makes 1D/2D hybrid materials promising for flexible electronics, sensors, transistors and next-generation electrode systems.[35] 1D/2D hybrid materials overcome the limitations of each dimensionality. 1D materials often suffer from poor film uniformity, weak mechanical integrity and high resistance at wire-to-wire junctions. Meanwhile, 2D nanosheets tend to restack due to van der Waals interactions, reducing available surface area and impairing out-of-plane conductivity. Incorporating 1D elements such as CNTs or metal nanowires between 2D layers prevents restacking and creates continuous multidimensional charge transport channels. The 2D layers, in turn, offer mechanical reinforcements and improved load distribution, preventing fracture of 1D networks during bending or stretching. Interfaces between 1D and 2D components can be chemically tuned to enhance electron mobility, charge separation and optoelectronic coupling, which are essential for sensors, transistors and photodetectors.[36] These hybrid structures have been applied across a wide range of electronic devices. CNT/graphene hybrids have been used as transparent, flexible electrodes for wearable electronics and foldable displays, where the unmined network provides high conductivity and mechanical robustness. MXene-CNT hybrids offer improved charge transport and flexibility, making them suitable for supercapacitors, micro-batteries, and conductive films.[37] MoS_2 nanosheets combined with silver or ZnO nanowires have been used in high-performance photoelectrodes and flexible field-effect transistors, where the hybrid interfaces accelerate

charge extraction. Graphene-ZNO nanowire architectures serve in UV detectors and electron-transport layers for optoelectronics. These examples illustrate the versatility of 1D/2D hybrids in enabling next-generation electronic platforms due to their outstanding flexibility, electronic transport behaviour and structural resilience.

2. Characterisation

2.1 UV-Visible Spectroscopy (UV-Vis)

UV-Vis spectroscopy measures the adsorption of ultraviolet and visible light of materials to study electronic transitions between molecular orbitals.[38] When photons in the 200-800 nm range strike a sample, electrons are excited from bonding (π or n) orbitals to anti-bonding (π* or σ*) orbitals. The amount of absorbed light follows Beer-Lambert's law ($A = \varepsilon cl$), where absorbance is proportional to concentration **(Figs. 2(a) and 2(b))**. The resulting absorption spectrum displays peaks corresponding to specific electronic transitions, providing information on molecular structure, band gaps, and concentration of absorbing species. In solid materials and nanostructures, UV-Vis spectroscopy is used to determine optical band gaps by analysing the absorption edge using Tauc plots. The technique is simple, rapid and suitable for liquids, solids, and colloids, often used in combination with diffuse reflectance setups. Applications include studying semiconductors, metal nanoparticles, dyes, and organic molecules. Although it lacks structural resolution, UV-Vis spectroscopy is an indispensable tool for probing optical and electronic properties and monitoring chemical reactions in real time.

2.2 Fourier Transform Infrared Spectroscopy (FTIR)

FTIR is a molecular characterisation method that identifies chemical bonds and functional groups based on infrared absorption.[38] When IR radiation interacts with a material, specific frequencies corresponding to bond vibrations are absorbed, producing characteristic peaks. The instrument employs a Michelson interferometer that splits and recombines IR light to generate an interferogram, which is mathematically converted (via Fourier transform) into an IR spectrum. Each absorption band corresponds to a vibrational mode, such as stretching or bending of molecular bonds, providing a unique chemical fingerprint**. Figs. 2(c) and 2(d)** illustrate the instrument and the basic working principle of FTIR. The technique can operate in transmission, reflection, or Attenuated Total Reflectance (ATR) modes, allowing analysis of solids, liquids and thin films. FTIR is widely used for identifying organic compounds, polymers, and surface functionalization in nanomaterials. It helps detect impurities, monitor

polymerisation, and study adsorption or reaction intermediates. While FTIR is highly informative, it is less effective for very thin layers and complex mixtures with overlapping peaks. Nonetheless, due to its simplicity, reproducibility and non-destructive nature, FTIR remains a vital tool in analytical chemistry, polymer science, and material characterisation.

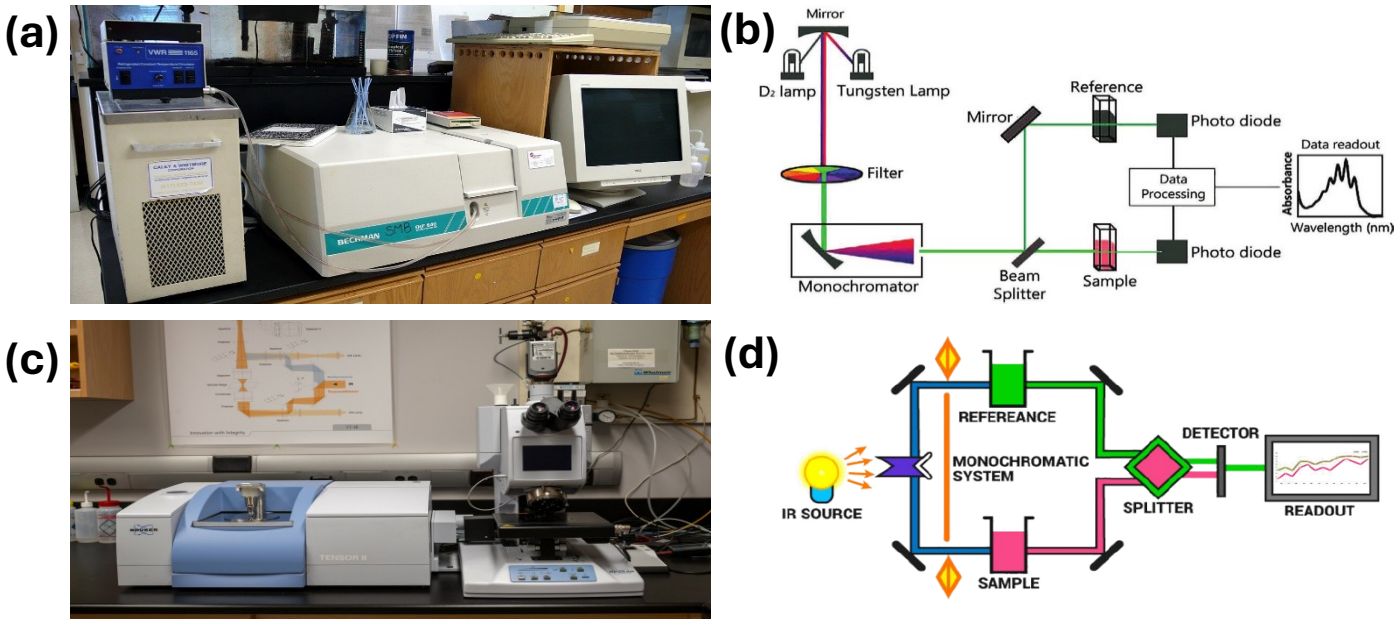

Fig. 2 (a) UV-visible spectroscope, **(b)** Principle of a UV-visible spectroscopy, **(c)** FTIR instrument, **(d)** Principle of FTIR

2.3 X-ray Diffraction (XRD)

XRD is a non-destructive fundamental technique for determining the crystal structure and phase composition of crystalline materials. The instrument and the basic operation principle are shown in **Figs. 3(a) and 3(b),** respectively. When a beam of monochromatic X-rays interacts with a periodic crystal lattice, constructive interference occurs at specific angles according to Bragg's law ($n\lambda = 2d \sin\theta$).[39] Measuring these diffraction angles and intensities produces a pattern unique to the crystal structure. The resulting diffractogram, plotted as intensity versus 2θ, provides interplanar spacings (d-values) and lattice parameters. XRD can identify crystalline phases by comparing experimental data to standard reference patterns from the International Centre for Diffraction Data (ICDD) database.[40] The technique also allows estimation of crystalline size using the Scherrer equation and quantitative phase analysis through Rietveld refinement. XRD is essential for studying materials such as ceramics, metals, and semiconductor structures, as well as layered 2D materials like graphene and MoS_2. It reveals

structural defects, preferred orientations, and phase transformations during synthesis or heat treatment. While less effective for amorphous samples and limited to bulk information, XRD remains one of the most reliable and widely used tools for structural characterisation.

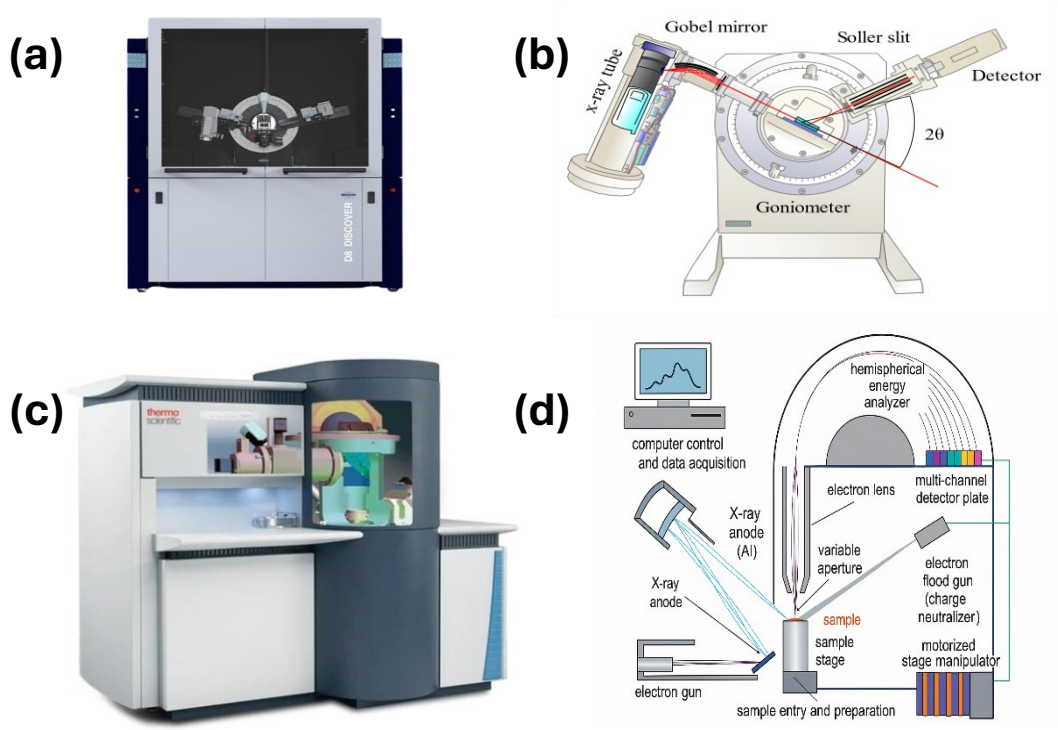

Fig. 3 (a) XRD instrument, **(b)** Principle representation of XRD, **(c)** XPS equipment, **(d)** Illustration of XPS process

2.4 X-ray Photoelectron Spectroscopy (XPS)

XPS is a surface-sensitive analytical technique that provides quantitative information about elemental composition and chemical states within the top few nanometers of a material. It is based on the photoelectric effect, where monochromatic (Al Kα or Mg Kα) eject core electrons from atoms. By measuring the kinetic energy of emitted electrons, the binding energy is calculated, which identifies each element and its oxidation state. The technique is extremely sensitive to surface chemistry and can distinguish between different chemical environments through small shifts in binding energy (**Figs. 3 (c) and 3(d)).** Depth profiling can be achieved by ion sputtering, enabling analysis of multilayer or coated systems. Counts per second is widely used to study surface contaminations, oxidation, thin film interfaces, and catalyst surfaces. It is particularly valuable for evaluating chemical bonding and charge transfer phenomena in functional materials. Although XPS requires vacuum operation and careful

sample handling, it offers unparalleled insight into surface composition and electronic structure, making it a cornerstone technique in surface science and nanomaterial research.

2.5 Electron Microscopy

(a) Scanning Electron Microscopy (SEM)

SEM is one of the most commonly used techniques for surface morphology and microstructural analuýsis of materials. SEM allows researchers to visualise the topography and composition of samples with nanometer-scale resolution. In SEM, a finely focused beam of high-energy electrons (1-40keV) scans the sample's surface inside a high vacuum chamber ($<10^{-4}$-10^{-5} Torr).[41] The electrons interact with atoms near the sample surface, resulting in the emission of the various signals, such as secondary electrons (SE), backscattered electrons (BSE), and characteristic X-rays. SEs, generated from the outermost layers, are primarily used to produce detailed topographical images that reveal the fine surface features. BSEs, which originate from the deeper regions of the sample, are more sensitive to atomic number contrast and are thus used to distinguish between phases of different compositions.[42] The intensity of BSEs increases with atomic number, which helps identify heavier elements. Additionally, the X-rays emitted during electron-atom interactions can be detected through energy-dispersive X-ray spectroscopy (EDS), providing qualitative and semi-quantitative elemental composition data.[43] The principle of SEM is based on the interaction volume **(Fig. 4 (b))**, which depends on the beam energy and the atomic number of the sample.[42] Conductive samples produce high-quality images directly, while non-conductive samples require coating with a conductive layer (gold, carbon or platinum) to prevent surface charging.[44] The electron beam is raster-scanned across the surface using electromagnetic lenses, and the resulting signals are converted into a digital image. SEM is versatile and applicable to a wide range of materials, including metals, ceramics, polymers, semiconductors, and biological tissues.[45]

SEM can be used to study surface texture, particle size, fracture patterns, and phase distributions. It can also identify defects and morphological features that influence material performance. The modern field-emission SEM systems offer resolution below 10 nm and support magnifications ranging from a few hundred to several hundred thousand times (>300000x).[46] However, the technique requires vacuum compatibility, and insulating samples may suffer from charging artefacts or beam-induced damage. Despite these limitations, SEM remains a cornerstone of material characterisation due to its ability to correlate structural,

morphological, and compositional information, making it indispensable for microstructural analysis, quality control, and nanotechnology research.

(b) Transmission Electron Microscopy (TEM)

TEM provides atomic-scale structural information by transmitting a high-energy electron beam through an ultrathin specimen, typically less than 100 nm thick[47] As the electrons interact with the atoms, they scatter elastically and inelastically, forming images and diffraction patterns that reveal both morphology and crystallinity **(Fig. 4 (a)).**[48] The image contrast arises from differences in mass thickness, diffraction, or phase of the transmitted electron. High-resolution TEM (HRTEM) enables direct visualisation of atomic lattices, while Selected Area Electron Diffraction (SAED) provides precise crystallographic information. The principle is based on the wave nature of electrons, allowing atomic-scale imaging due to their short de Broglie wavelength.[49] TEM often integrates analytical techniques such as EDS and Electron Energy Loss Spectroscopy (EELS) for simultaneous elemental mapping.[49], [50] Preparing electron-transparent specimens is a critical and challenging step, often involving ion milling or microtoming.[48] TEM is invaluable for studying nanomaterials, interfaces, dislocations, and phase transformations in metals, semiconductors, and oxides. Although costly and technically demanding, it remains the most powerful tool for correlating microstructure with material properties at the atomic level.[47], [49]

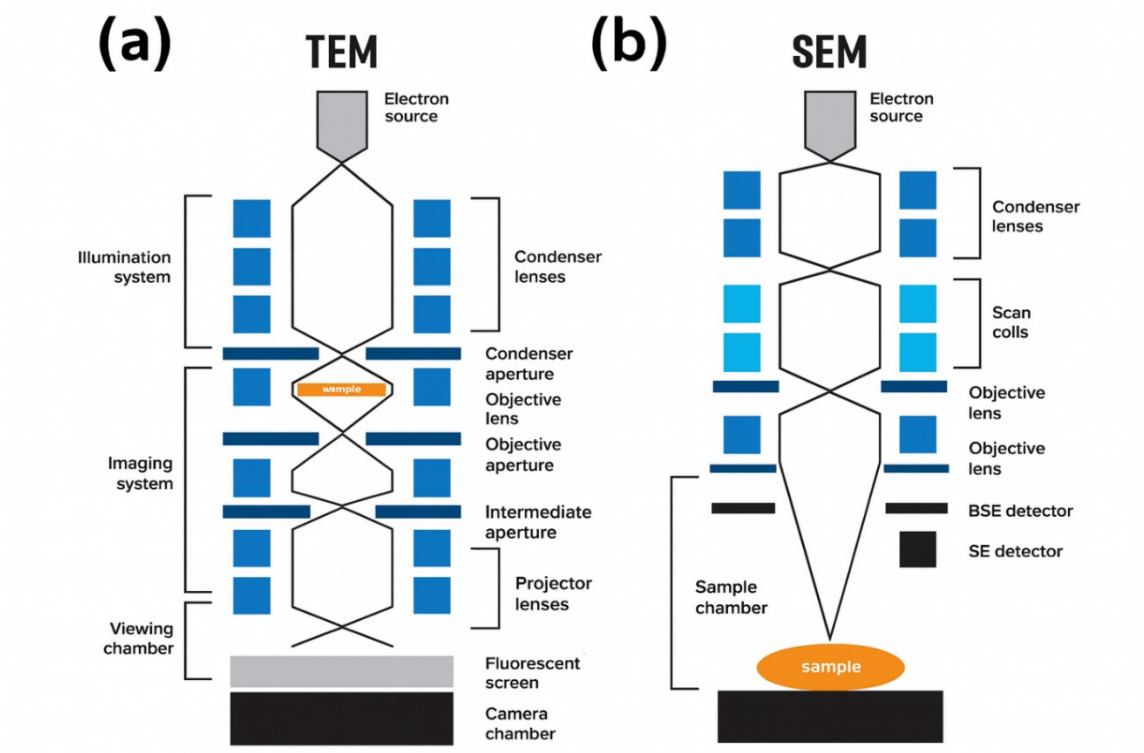

Fig. 4 Principle of **(a)** TEM and **(b)** SEM

3. Experimental Section

3.1 Materials and Reagents

Copper (II) chloride dihydrate ($CuCl_2.2H_2O$, ACS reagent), Hexadecylamine (HDA, approximate C-18 content 80 – 90%), D+- glucose (≥99%, analytical reagent grade) were purchased from Fisher Scientific. Propionic acid (≥99%, laboratory reagent grade) was purchased from Merck (Sigma-Aldrich). Ethanol was purchased from Anora Group Oy, and deionised water was obtained from a PuroTM reverse osmosis water purifier from Avidity Science, MAX phase, Hydrochloric acid (HCl), Lithium fluoride (LiF), Lithium chloride (LiCl).

3.2 Synthesis of Copper Nanowires (CuNWs)

CuNWs were synthesised according to a previously reported procedure with some modifications. [1] Briefly, $Cu(II)Cl_2.2H_2O$ (85 mg, 0.5 mmol), glucose (207.5 mg, 1.05 mmol), Hexadecylamine (HDA, 665 mg, 2.25 mmol), and deionised water (40 mL, 18.25 MΩ) were added to a glass beaker and stirred vigorously at room temperature for 5 h to form a homogeneous solution. The mixture was then transferred to a 100 mL Teflon-lined autoclave, which was later sealed inside a stainless-steel autoclave case. Further, the reaction container was heated at 110 °C for 12 h without further agitation. The resulting reddish-brown-coloured reaction mixture containing CuNWs was cleaned using ethanol and propionic acid. The process involves, firstly, cleaning three times with ethanol to remove residual HDA and glucose, afterwards once with PA to clean the carbon residues which are on the nanowire's surface and later twice with ethanol to remove residual PA (presence of which may lead to faster degradation of CuNWs) **(Fig. 5 (a))**. The cleaning process is conducted using a centrifuge at 6000 rpm for 5 min. Between cleaning cycles, the reaction mixture was agitated using pipettes to maintain the dispersibility of CuNWs. The final product was dispersed in ethanol (40 mL) for subsequent characterisation and film fabrication.

3.3 Synthesis of MXene

Titanium-based MXene was also synthesised based on a previously published report with minute modifications to the process.[51] To explain briefly, MXene was prepared via an in situ etching process of alumina from the MAX phase Ti_3AlC_2, utilising the in situ formation of HF with LiF/HCl. system. Briefly, 1.2 g of LiF (2.3 M) was dissolved in 20 mL of 12 M HCl in a PTFE container and stirred for 10 min to obtain a homogeneous solution. Followed by the slow addition of 1 g of Ti_3AlC_2 powder (450 mesh). The mixture was stirred using a PTFE-coated

magnetic stir bar at 1500 rpm for 24 hours at 35 °C. After etching, the resulting mixture was washed once with 40 mL of 1 M HCl and subsequently three times with 40 mL of 1 M LiCl solution. The multilayered MXene was then washed three more times with 40 mL of deionised (DI) water. For each wash, 40 mL of DI water was transferred into a centrifuge tube, shaken by hand for 1 minute, and centrifuged at 4020 rcf for 2 minutes, after which the supernatant was decanted. The resulting supernatant was decanted, and 50 mL of fresh DI water was added to the precipitate. Following the final wash, the mixture was agitated using a bath sonicator for 1 hour, while keeping the temperature between 20-25 °C, keeping the MXene from degradation. Finally, the reaction mixture was centrifuged at 2060 rcf for 1 hour to separate Heavier multilayered MXene from lighter single to few-layered MXene sheets. The resulting supernatant, containing single to few-layer $Ti_3C_2T_x$ flakes, had a concentration of approximately 4-4.5 mg/mL. The resulting solution was purged using a nitrogen environment and was kept in the dark at a low temperature (< 5°C) for future use **(Fig. 5 (b))**.

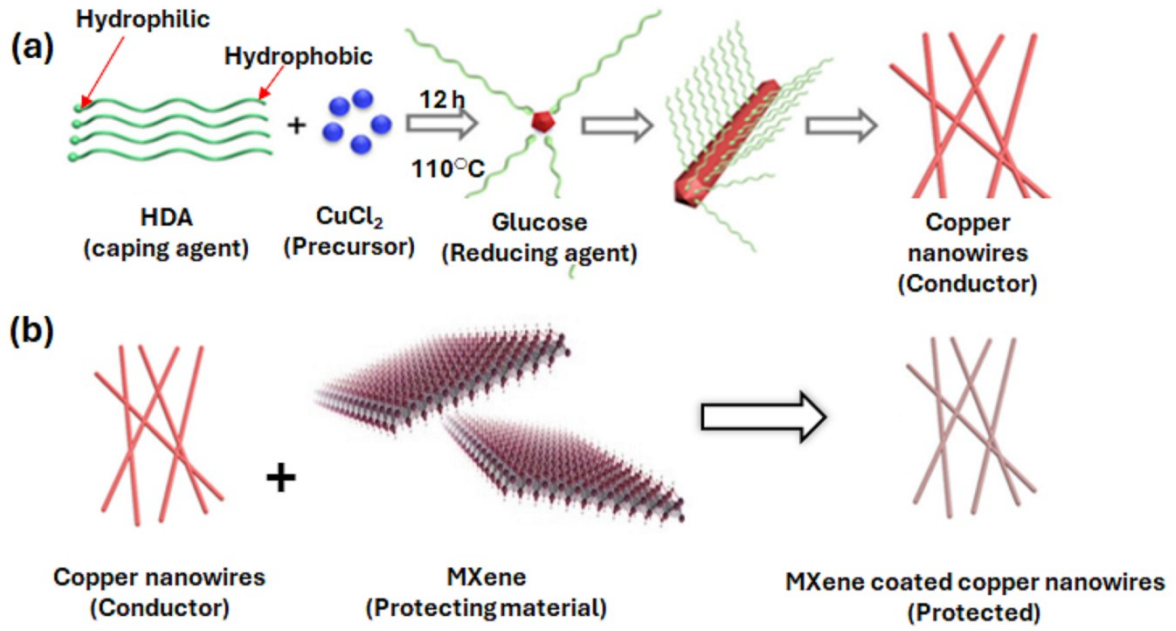

Fig. 5 Synthesis process of **(a)** 1D CuNWs, **(b)** 2D MXene

3.4 Synthesis of CuNWs-MXene Composite Nanowires (Cu-MXene)

To prepare Cu-MXene composite nanowires, a 1:1 volume ratio of 5 mL CuNW suspension (0.1 mg mL^{-1}) and ethanol was prepared. Separately, 0.250 mL of MXene suspension (0.5 mg/mL) was sonicated for 30 minutes to obtain a well-dispersed MXene solution. The diluted CuNWs solution was then added to the MXene solution, and the resulting solution was degassed

by purging with nitrogen gas for 10 minutes. The mixture was kept in a refrigerator (< 5 °C) for 30 minutes to facilitate physisorption. The resulting product was used to prepare further samples for characterisation.

4 Results and Discussion

4.1 Characterisation Techniques

To characterise our samples following characterisation techniques were used: Initial confirmation for the successful material synthesis was done using UV-Vis spectroscopy, and X-ray diffraction (XRD) was conducted using a Panalytical Empyrean X-ray diffractometer using a PIXcel3D solid state area detector. The analysis range was chosen from the 2θ values 30-80° at a scan rate of 2° min^{-1}. A Thermo Scientific Nexsa instrument conducted X-ray photoelectron spectroscopy (XPS). Morphological analysis of the fabricated CuNWs was conducted using a field-emission scanning electron microscope (FE-SEM) (Apreo S, Thermofisher Scientific) at an operating voltage of 2 kV. A high-resolution transmission electron microscope (HRTEM) (Jeol JEM-F200, Ver 4) was also used for CuNW morphological analysis, at an operating voltage of 200 kV. The sheet resistance of the TCEs was measured using an Ossila four-point probe system, which features a probe spacing of 1.27 mm.

4.2 Results and Discussion

Durable nanowires were prepared by encapsulating individual copper nanowires suspended in solution. The ultra-long copper nanowires were synthesised via a hydrothermal approach. The average diameter of the nanowire measured is ~ 60 nm. Furthermore, Cu-MXene composite nanowires were prepared by mixing CuNWs and an MXene solution in ethanol at room temperature. Copper nanowires have high surface energy. Due to the highly reactive functional groups at the MXenes basal plane, which were maintained under a nitrogen atmosphere and at a low temperature (<5 ℃).

SEM analysis and TEM analysis were conducted to characterise the structural identity and morphology change of the Cu-MXene nanowires, and electron micrographs were acquired. The CuNWs were prepared via the HAD-mediated hydrothermal method. In this process, $CuCl_2.2H_2O$ was reduced using glucose. HDA was used as a capping agent to control the asymmetrical, unidirectional growth of 1D nanowires. From the SEM analysis **(Fig. 7 (a)),** the average diameter of CuNWs was measured at 60 ± 0.3 nm, and they are >100 μm long. On the

other hand, the MXene nanosheets have large 2D structures their corresponding morphologies are shown in **Fig. 7 (b)**. Cu-MXene composite nanowires were synthesised at room temperature. TEM was conducted to analyse the interface and morphology of the Cu-MXene composite nanowires, as shown in **Fig. 7 (e)**.

Fig. 6 (a) Comparative XRD plot of MXene, CuNWs and Cu-MXene composite nanowires**, (b)** relative

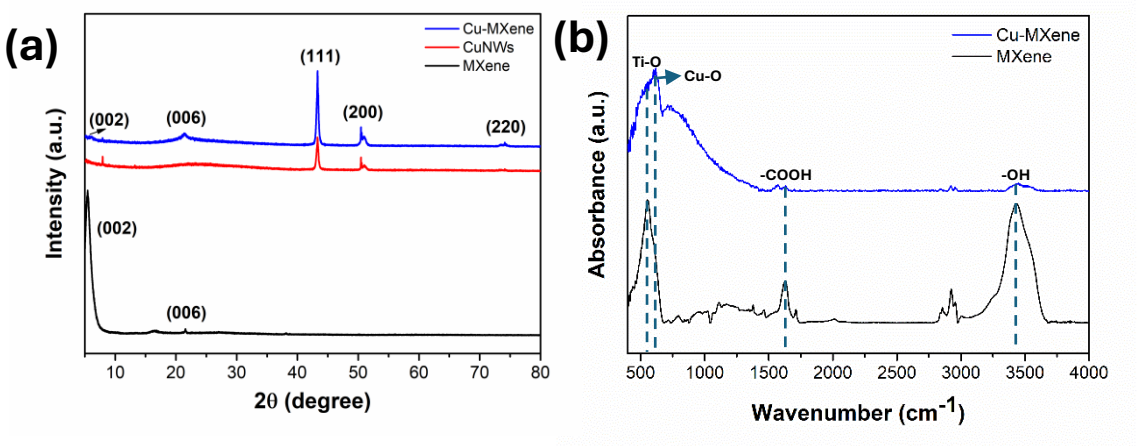

FTIR analysis of MXene and Cu-MXene

To determine the crystalline phases and crystal structure of the as-prepared CuNWs and MXene, XRD analysis is used, as shown in **Fig. 6 (a)**. The CuNWs exhibit three characteristic peaks at 2θ values 43.3º, 50.4º, and 74.1º corresponding to the (111), (200), and (220) crystal planes, respectively.[1] In the case of Cu-MXene NWs, an additional diffraction peak corresponding to the (002) plane of MXene is observed, confirming the presence of both materials in their respective crystalline forms (**Fig. 6 (a)**).

To further investigate the chemical interaction between CuNWs and MXene, FTIR spectra were obtained **(Fig. 6 (b)).** MXene shows distinct vibrational modes at 3439.8 and 1630.7 cm^{-1}, attributed to the stretching and bending vibrations of –OH and -COOH groups, respectively.[52] These modes are significantly reduced or absent in Cu-MXene NWs, indicating surface modification. Moreover, Cu-MXene NWs exhibit a new stretching vibration at 598.8 cm^{-1}, suggesting the formation of Cu–O bonds. Both MXene and Cu-MXene NWs exhibit a common vibrational band at lower wavenumbers (553.5 cm^{-1}), indicating a strong interfacial interaction in the Cu-MXene nanowire structure.

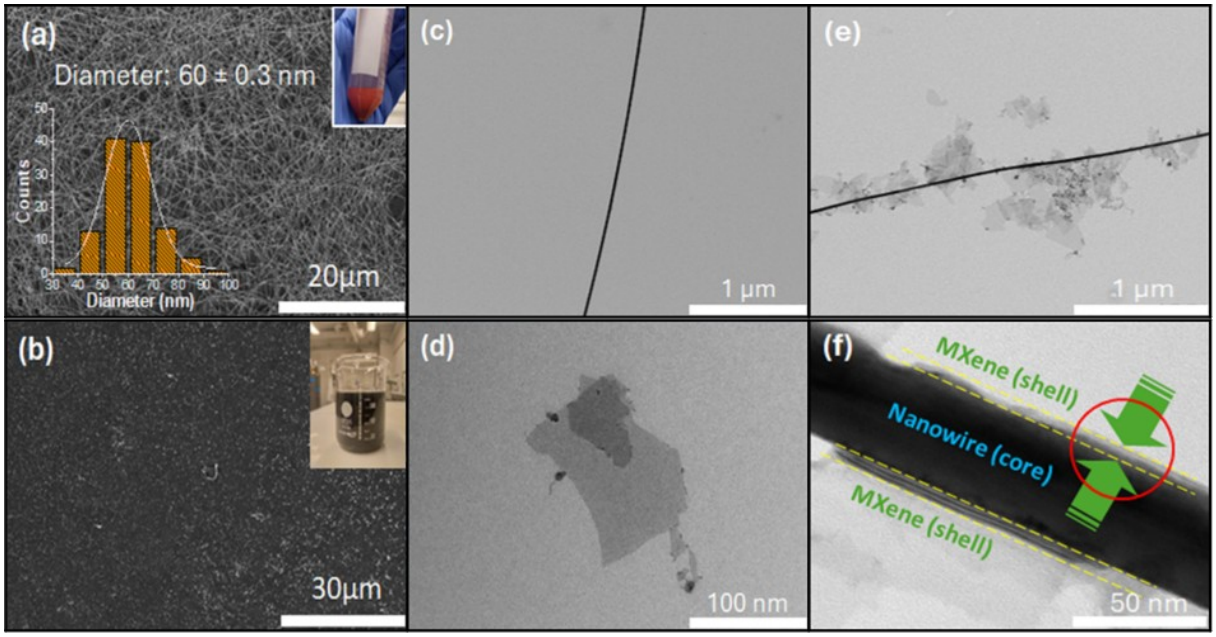

Fig.7 SEM images **(a)** CuNWs with a diameter of 60 ± 0.3 nm, **(b)** single to few sheets of MXene, TEM images of (**c)** a single CuNW, **(d)** Single to few sheets of MXene, **(e)** interaction between CuNW and MXene in Cu-MXene hybrid, **(f)** closeup of Cu-MXene composite nanowires illustrating the successful interaction between CuNW and MXene

To understand the surface properties and purity of the nanomaterials, XPS analysis was conducted. From the survey spectra, the elemental composition of Cu-MXene NWs was compared with that of pristine MXene and CuNWs. The Cu-MXene nanowires primarily consist of Cu, Ti, C, and O elements, confirming the coexistence of both MXene and copper components. High-resolution spectra for the Cu2p and O1s regions were acquired to examine surface interactions **(Fig. 8 (c) and 8 (d)).** The O1s spectrum of MXene was deconvoluted using a Shirley background and showed four main components at ≈ 530.5, ≈ 531.2, ≈ 532.0, and ≈ 533.5 eV, corresponding to C–Ti–O_x, Ti–O–Ti, C–Ti–$(OH)_x$, and adsorbed oxygen, respectively. These indicate that the MXene surface is predominantly terminated with –OH functional groups. Interestingly, in Cu-MXene NWs, an additional peak appears at a lower binding energy (≈529.8 eV), indicating the formation of Cu-O bonds, which suggests a strong interaction at the Cu-MXene interface. The Cu 2p spectrum **(Fig. 8 (c))** shows a characteristic spin-orbit doublet at 952.6 eV (Cu $2p_{1/2}$) and 932.8 eV (Cu $2p_{3/2}$), separated by 19.8 eV with an intensity ratio of 1:2, confirming the presence of metallic copper in the Cu-MXene NWs.[53] Notably, no satellite peaks were observed, which typically indicate the presence of Cu^{+} or Cu^{2+} oxidation states. The results reveal that Cu^{0} is the predominant oxidation state, while Cu^{+} is present in smaller amounts. This confirms that the copper in the Cu-MXene NWs is primarily

in the metallic state, with minimal oxidation. Moreover, the C1s spectrum of Cu-MXene NWs (**Fig. 8 (a)**) shows a Ti-C interaction at 281.5 eV, with a noticeable shift toward lower binding energy compared to pure MXene. Additionally, the Ti2p spectrum of Cu-MXene displays characteristic peaks of MXene, at 454.6, 455.6, and 457.5 eV corresponding to Ti-X (Ti^{2+}), Ti-O (Ti^{3+}), and Ti-$(OH)_x$ (Ti^{4+}) as shown in **Fig. 8 (b)**.[52]

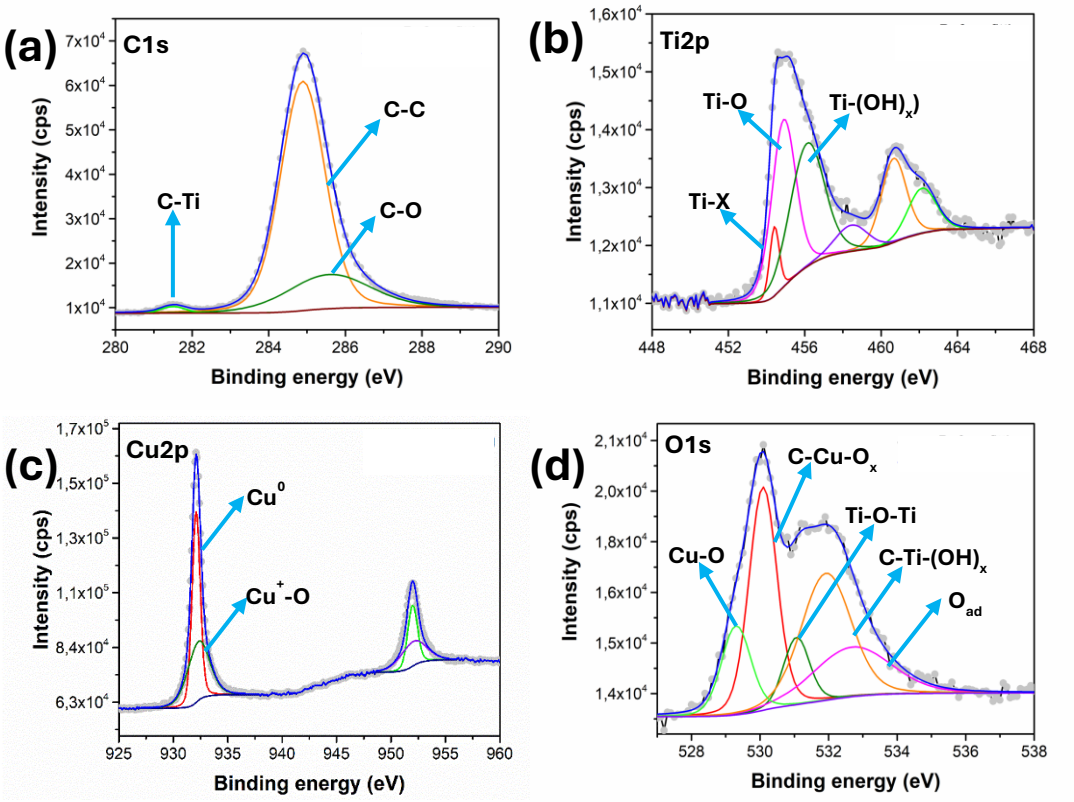

Fig. 8 XPS analysis representing **(a)** C1s, **(b)** Ti2p, **(c)** Cu2p, and **(d)** O1s plots

Further, the influence of MXene on CuNWs was investigated using UV-Vis absorbance spectroscopy. A comparative plot was made between bare Copper, bare MXene and composite material with different compositions of MXene, as shown in **Fig. 9 (a).** A broader peak in the NIR region (700-800 nm) confirms the formation of MXene. Copper nanowires exhibit localised surface plasmon resonance (LSPR), a light absorption phenomenon that depends on micromorphology, such as size and shape. To assess this, CuNWs were coated with varying concentrations of MXene, and the corresponding changes were analysed through their absorbance spectra. Typically, variations in nanowire diameter affect the position of the transverse LSPR peak. As shown in Subplot of **Fig. 9 (a)**, uncoated nanowires display a distinct transverse LSPR peak at 555 nm. Upon MXene coating, a noticeable redshift in the LSPR peak

was observed with increasing MXene concentration. This redshift suggests an increase in effective diameter, indicating strong interactions between the CuNWs and MXene.[54]

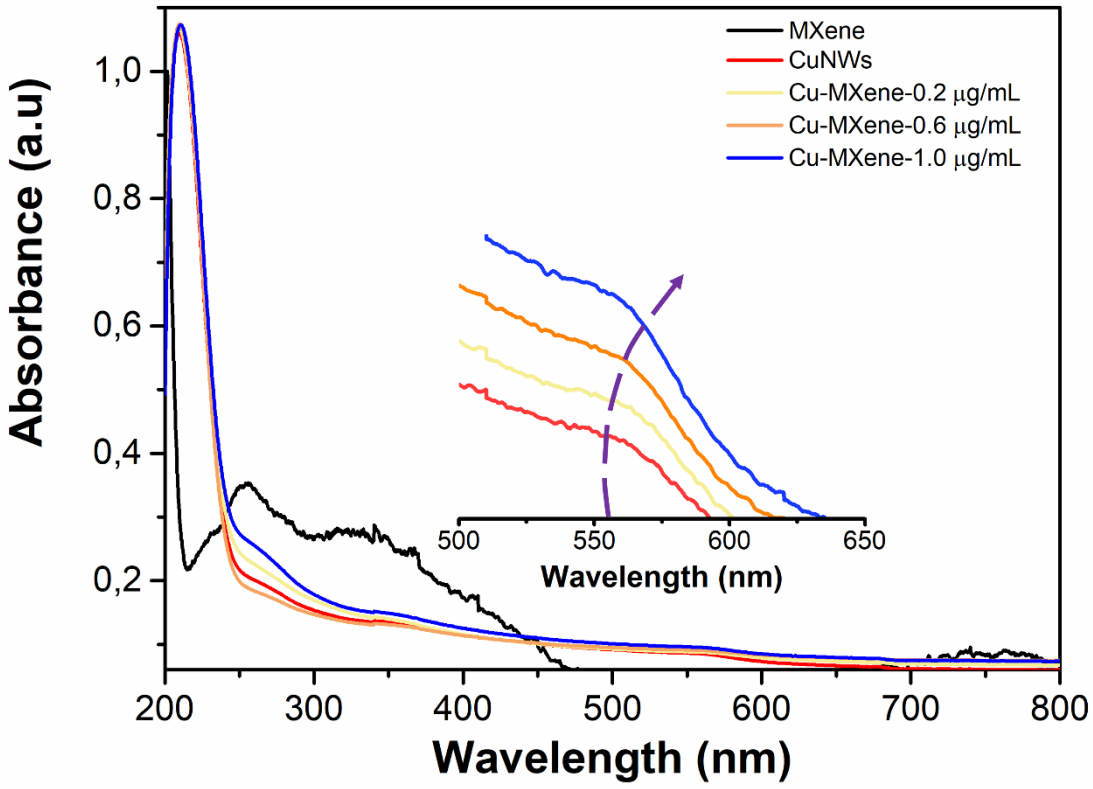

Fig. 9 (a) Comparative illustration of UV-vis spectroscopy plots of bare copper nanowires, MXene and Cu-MXene composite with three different compositions of MXene

4.2.1 Degradation Studies:

Initially, different concentrations of Cu-MXene composite nanowires were deposited on top of a cellulose-based filter paper to optimise the concentration of MXene. The concentration optimisation was based on the change in sheet resistance over 28 days, as illustrated in **Fig. 10 (a).** Additionally, a sample containing the highest MXene concertation from this experiment was prepared. However, it exhibited no measurable conductivity, likely due to insufficient interactions between the MXene nanostructures. The major conclusions that were derived from these observations (i) increasing the MXene content in the composite improves the stability but reduces the overall electrical conductivity of the composite nanowires, (ii) the addition of MXene effectively protects the CuNWs from oxidation, maintaining their structural integrity for over 28 days, and (iii) in the composite, the CuNWs are responsible for electrical conductivity, while MXene primarily provides protection against oxidation. Furthermore, two

different samples of Cu-MXene composite nanowires were prepared; ones ample was subjected to heat at 70 °C, and the sheet resistance data for both samples were taken for a period of 28 days. The sample subjected to heat exhibited better stability over time compared to the other sample, suggesting increased stability with temperature **(Fig. 10 (b))**.

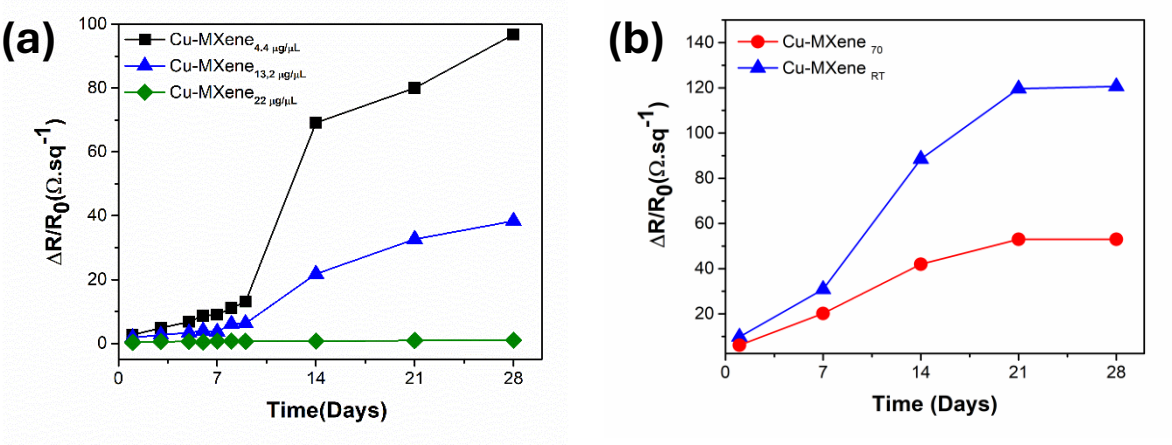

Fig. 10 Sheet resistance data for 28 days **(a)** varying MXene concentrations in Cu-MXene hybrid, **(b)** effect of temperature on Cu-MXene hybrid

During this study, various synthesis methods and characterisation techniques were employed to achieve our goals. The main research questions that we tried to tackle were (i) finding the interactions between 1D CuNWs and 2D MXene, (ii) whether the MXene coating is successfully incorporated on top of CuNWs, and (iii) whether it can increase the lifetime of CuNWs compared to other studies that have been done. The synthesis processes for both materials were conducted separately. CuNWs were prepared using a simple hydrothermal process while using glucose and hexadecyl amine as reducing agent and capping agent, respectively. This results in ultralong nanowires, which were confirmed using XRD and SEM and TEM techniques, to extract the morphological and topological information of the prepared CuNWs. Furthermore, MXene was prepared using an in situ etching method, in which HF was employed as an etchant to remove aluminium (Al) from the MAX phase (Ti_3AlC_2). The successful formation of MXene was confirmed using XRD, SEM and TEM. Furthermore, a one-step self-assembly method was used to produce a Cu-MXene hybrid; the success of the process was confirmed using XRD, SEM, TEM, and XPS.

After the material characterisation, degradation studies in the ambient conditions were conducted to verify the claim of increasing the longevity of CuNWs. During the process, the as-prepared Cu-MXene composite nanowires were deposited on top of a flexible substrate, and the stability of the material was determined via sheet resistance measurement for over 4 weeks.

5 Conclusion and Future Prospects

During the course of this work, a successful synthesis of 1D CuNWs was done using a simple hydrothermal process. This was further demonstrated using various characterisation techniques. For instance, XRD was employed to confirm the FCC crystal structure of CuNWs, which exhibited three prominent peaks corresponding to the (111), (200), and (220) crystal planes of copper nanowires, as confirmed via a literature review. Additionally, SEM was employed for a better view of the surface morphology of as-prepared CuNWs. SEM analysis revealed the formation of ultra-long nanowires with 60 ± 3 nm thickness, and they are about >100 nm long. This confirmed the successful formation of CuNWs. Furthermore, 2D Ti-based MXene ($Ti_3C_2T_X$) was synthesised using an in-situ HF etching method. The success of the process was confirmed by utilising XRD, SEM and TEM. XRD validates by showing characteristic peaks for (002), (004), (006) planes, which were verified via a literature review and a comparative XRD of MAX phase (Ti_3AlC_2) and the synthesised MXene ($Ti_3C_2T_X$). Later, Cu-MXene composite nanowires were formed via a self-assembly method, simply by mixing the solutions of CuNWs and MXene, which resulted in interactions between the CuNWs and MXene. To determine the success of the reaction again, TEM, FTIR and XPS were utilised. TEM revealed the formation of an uneven MXene coating on the surface of CuNWs, and XPS confirms the presence of Cu-O bond without the formation of oxides on the surface of nanowires, which confirms the active interaction between MXene functionalities and CuNWs surface. Lastly, the increased durability of the prepared material was tested under ambient conditions over a period of 28 days. This illustrates the increased durability of CuNWs after the formation of the Cu-MXene hybrid.

Despite promising results, achieving a uniform MXene coating on CuNWs remains challenging. Similar to previous research on Cu-graphene core/shell structures, achieving Cu-MXene core-shell structures could enhance mechanical properties, charge transfer, surface area, and functionalization, expanding their applications in nanoelectronics and photocatalysis.[55] Dealing with the uniformity problem will also enhance the transparency of the material, hence expanding the application horizon into optoelectronics. Additionally, prospects for further exploration include using smaller morphologies of MXene, as well as ultra-thin MXene sheets, to test stability under oxidising environments. Furthermore, light sensitivity and mechanical bending tests could provide deeper insights into their performance and applications.

6 References

[1] Q. Xie *et al.*, "Transparent, Flexible, and Stable Polyethersulfone/Copper-Nanowires/Polyethylene Terephthalate Sandwich-Structured Films for High-Performance Electromagnetic Interference Shielding," *Adv Eng Mater*, vol. 23, no. 8, p. 2100283, Aug. 2021, doi: 10.1002/ADEM.202100283.

[2] A. Aliprandi *et al.*, "Hybrid Copper-Nanowire–Reduced-Graphene-Oxide Coatings: A 'Green Solution' Toward Highly Transparent, Highly Conductive, and Flexible Electrodes for (Opto)Electronics," *Advanced Materials*, vol. 29, no. 41, p. 1703225, Nov. 2017, doi: 10.1002/ADMA.201703225.

[3] Z. Yang *et al.*, "MXene/AgNWs/MXene Sandwich-Structured Transparent Electrode for High-Performance Flexible OLEDs," *Small*, vol. 21, no. 14, Apr. 2025, doi: 10.1002/SMLL.202409621.

[4] D. S. Hecht and R. B. Kaner, "Solution-processed transparent electrodes," *MRS Bull*, vol. 36, no. 10, pp. 749–755, Oct. 2011, doi: 10.1557/MRS.2011.211/FIGURES/4.

[5] M. Morales-Masis, S. De Wolf, R. Woods-Robinson, J. W. Ager, and C. Ballif, "Transparent Electrodes for Efficient Optoelectronics," *Adv Electron Mater*, vol. 3, no. 5, p. 1600529, May 2017, doi: 10.1002/AELM.201600529.

[6] Y. Ding *et al.*, "Metal nanowire-based transparent electrode for flexible and stretchable optoelectronic devices," *Chem Soc Rev*, vol. 53, no. 15, pp. 7784–7827, Jul. 2024, doi: 10.1039/D4CS00080C.

[7] J. Wang, W. Piao, X. Jin, L. Y. Jin, and Z. Yin, "Recent Progress in Metal Nanowires for Flexible Energy Storage Devices," *Front Chem*, vol. 10, p. 920430, May 2022, doi: 10.3389/FCHEM.2022.920430.

[8] C. Y. Hsu *et al.*, "Nanowires Properties and Applications: A Review Study," *S Afr J Chem Eng*, vol. 46, pp. 286–311, Oct. 2023, doi: 10.1016/J.SAJCE.2023.08.006.

[9] J. Shi, M. Zhang, S. Ding, and G. Cao, "Recent Progress in Copper Nanowire-Based Flexible Transparent Conductors," *Coatings 2025, Vol. 15, Page 465*, vol. 15, no. 4, p. 465, Apr. 2025, doi: 10.3390/COATINGS15040465.

[10] S. Ding and Y. Tian, "Recent progress of solution-processed Cu nanowires transparent electrodes and their applications," *RSC Adv*, vol. 9, no. 46, pp. 26961–26980, Aug. 2019, doi: 10.1039/C9RA04404C.

[11] A. Aliprandi *et al.*, "Hybrid Copper-Nanowire–Reduced-Graphene-Oxide Coatings: A 'Green Solution' Toward Highly Transparent, Highly Conductive, and Flexible Electrodes for (Opto)Electronics," *Advanced Materials*, vol. 29, no. 41, p. 1703225,

Nov. 2017, doi: 10.1002/ADMA.201703225;REQUESTEDJOURNAL:JOURNAL:15214095;WGROUP:STRING:PUBLICATION.

[12] A. T. Bellew, H. G. Manning, C. Gomes da Rocha, M. S. Ferreira, and J. J. Boland, "Resistance of Single Ag Nanowire Junctions and Their Role in the Conductivity of Nanowire Networks," *ACS Nano*, vol. 9, no. 11, pp. 11422–11429, Nov. 2015, doi: 10.1021/ACSNANO.5B05469.

[13] "High performing AgNW transparent conducting electrodes with a sheet resistance of 2.5 Ω Sq −1 based upon a roll-to-roll compatible post-processing tec ... - Nanoscale (RSC Publishing) DOI:10.1039/C8NR07974A." Accessed: Nov. 11, 2025. [Online]. Available: https://pubs.rsc.org/en/content/articlehtml/2017/sc/c8nr07974a

[14] Y. Ahn, Y. Jeong, and Y. Lee, "Improved thermal oxidation stability of solution-processable silver nanowire transparent electrode by reduced graphene oxide," *ACS Appl Mater Interfaces*, vol. 4, no. 12, pp. 6410–6414, Dec. 2012, doi: 10.1021/AM301913W.

[15] V. Shanmugam *et al.*, "A Review of the Synthesis, Properties, and Applications of 2D Materials," *Particle & Particle Systems Characterization*, vol. 39, no. 6, p. 2200031, Jun. 2022, doi: 10.1002/PPSC.202200031.

[16] N. R. Glavin, C. Muratore, and M. Snure, "Toward 2D materials for flexible electronics: opportunities and outlook," *Oxford Open Materials Science*, vol. 1, no. 1, Nov. 2020, doi: 10.1093/OXFMAT/ITAA002.

[17] J. Park, J. C. Hwang, G. G. Kim, and J. U. Park, "Flexible electronics based on one-dimensional and two-dimensional hybrid nanomaterials," *InfoMat*, vol. 2, no. 1, pp. 33–56, Jan. 2020, doi: 10.1002/INF2.12047.

[18] W. Chen *et al.*, "A 1D:2D structured AgNW:MXene composite transparent electrode with high mechanical robustness for flexible photovoltaics," *J Mater Chem C Mater*, vol. 10, no. 22, pp. 8625–8633, Jun. 2022, doi: 10.1039/D2TC01178F.

[19] Y. Zhong *et al.*, "Interface engineering of heterojunction photocatalysts based on 1D nanomaterials," *Catal Sci Technol*, vol. 11, no. 1, pp. 27–42, Jan. 2021, doi: 10.1039/D0CY01847C.

[20] N. Fu *et al.*, "High-Sensitivity 2D MoS2/1D MWCNT Hybrid Dimensional Heterostructure Photodetector," *Sensors 2023, Vol. 23, Page 3104*, vol. 23, no. 6, p. 3104, Mar. 2023, doi: 10.3390/S23063104.

[21] X. Long, L. Zhang, Z. Tan, and B. Zhou, “Progress on 2D–2D heterostructured hybrid materials for efficient electrocatalysis,” *Energy Advances*, vol. 2, no. 2, pp. 280–292, Feb. 2023, doi: 10.1039/D2YA00318J.

[22] H. H. S. Thangavelu, C. Huang, F. Chabanais, J. Palisaitis, and P. O. Å. Persson, “A Review on MXene Terminations,” *Adv Funct Mater*, 2025, doi: 10.1002/ADFM.202515604.

[23] B. Mekuye and B. Abera, “Nanomaterials: An overview of synthesis, classification, characterization, and applications,” *Nano Select*, vol. 4, no. 8, pp. 486–501, Aug. 2023, doi: 10.1002/NANO.202300038.

[24] H. D. Yu, M. D. Regulacio, E. Ye, and M. Y. Han, “Chemical routes to top-down nanofabrication,” *Chem Soc Rev*, vol. 42, no. 14, pp. 6006–6018, Jun. 2013, doi: 10.1039/C3CS60113G.

[25] P. Wang, C. Jia, Y. Huang, and X. Duan, “Van der Waals Heterostructures by Design: From 1D and 2D to 3D,” *Matter*, vol. 4, no. 2, pp. 552–581, Feb. 2021, doi: 10.1016/J.MATT.2020.12.015.

[26] G. Badawy and E. P. A. M. Bakkers, “Electronic Transport and Quantum Phenomena in Nanowires,” *Chem Rev*, vol. 124, no. 5, pp. 2419–2440, Mar. 2024, doi: 10.1021/ACS.CHEMREV.3C00656.

[27] S. W. Eaton, A. Fu, A. B. Wong, C. Z. Ning, and P. Yang, “Semiconductor nanowire lasers,” *Nat Rev Mater*, vol. 1, no. 6, pp. 16028-, May 2016, doi: 10.1038/NATREVMATS.2016.28;SUBJMETA.

[28] H. Wang, M. Sun, K. Ding, M. T. Hill, and C. Z. Ning, “A Top-down Approach to Fabrication of High Quality Vertical Heterostructure Nanowire Arrays,” *Nano Lett*, vol. 11, no. 4, pp. 1646–1650, Apr. 2011, doi: 10.1021/NL2001132.

[29] H. D. Yu, M. D. Regulacio, E. Ye, and M. Y. Han, “Chemical routes to top-down nanofabrication,” *Chem Soc Rev*, vol. 42, no. 14, pp. 6006–6018, Jun. 2013, doi: 10.1039/C3CS60113G.

[30] G. Badawy and E. P. A. M. Bakkers, “Electronic Transport and Quantum Phenomena in Nanowires,” *Chem Rev*, vol. 124, no. 5, pp. 2419–2440, Mar. 2024, doi: 10.1021/ACS.CHEMREV.3C00656.

[31] X. Cai, Y. Luo, B. Liu, and H. M. Cheng, “Preparation of 2D material dispersions and their applications,” *Chem Soc Rev*, vol. 47, no. 16, pp. 6224–6266, Aug. 2018, doi: 10.1039/C8CS00254A.

[32] L. Liu, W. An, F. Gu, L. Cui, X. He, and M. Fan, “2D layered materials: structures, synthesis, and electrocatalytic applications,” *Green Chemistry*, vol. 25, no. 16, pp. 6149–6169, Aug. 2023, doi: 10.1039/D3GC01822A.

[33] J. Yu, J. Li, W. Zhang, and H. Chang, “Synthesis of high quality two-dimensional materials via chemical vapor deposition,” *Chem Sci*, vol. 6, no. 12, pp. 6705–6716, Nov. 2015, doi: 10.1039/C5SC01941A.

[34] Y. Shi, H. Li, and L. J. Li, “Recent advances in controlled synthesis of two-dimensional transition metal dichalcogenides via vapour deposition techniques,” *Chem Soc Rev*, vol. 44, no. 9, pp. 2744–2756, Apr. 2015, doi: 10.1039/C4CS00256C.

[35] B. Vedhanarayanan, V. K. Praveen, G. Das, and A. Ajayaghosh, “Hybrid materials of 1D and 2D carbon allotropes and synthetic π-systems,” *NPG Asia Materials 2018 10:4*, vol. 10, no. 4, pp. 107–126, Apr. 2018, doi: 10.1038/s41427-018-0017-6.

[36] W. Wang *et al.*, “Mixed-Dimensional Anti-ambipolar Phototransistors Based on 1D GaAsSb/2D MoS2 Heterojunctions,” *ACS Nano*, vol. 16, no. 7, pp. 11036–11048, Jul. 2022, doi: 10.1021/ACSNANO.2C03673.

[37] N. Baig, I. Kammakakam, W. Falath, and I. Kammakakam, “Nanomaterials: a review of synthesis methods, properties, recent progress, and challenges,” *Mater Adv*, vol. 2, no. 6, pp. 1821–1871, Mar. 2021, doi: 10.1039/D0MA00807A.

[38] S. Sharma, D. Verma, L. Khan, S. Kumar, and S. Khan, *Handbook of materials characterization*. 2018. Accessed: Oct. 17, 2025. [Online]. Available: https://link.springer.com/content/pdf/10.1007/978-3-319-92955-2.pdf

[39] W. L. Bragg, “The diffraction of short electromagnetic Waves by a Crystal,” 1929. Accessed: Nov. 11, 2025. [Online]. Available: https://philpapers.org/rec/BRATDO-17

[40] S. N. Kabekkodu, A. Dosen, and T. N. Blanton, “PDF-5+: a comprehensive Powder Diffraction File™ for materials characterization,” *Powder Diffr*, vol. 39, no. 2, pp. 47–59, Jun. 2024, doi: 10.1017/S0885715624000150.

[41] T. E. Davies, H. Li, S. Bessette, R. Gauvin, G. S. Patience, and N. F. Dummer, “Experimental methods in chemical engineering: Scanning electron microscopy and X-ray ultra-microscopy—SEM and XuM,” *Can J Chem Eng*, vol. 100, no. 11, pp. 3145–3159, Nov. 2022, doi: 10.1002/CJCE.24405.

[42] W. Zhou, R. P. Apkarian, Z. Lin Wang, and D. Joy, “Fundamentals of Scanning Electron Microscopy”.

[43] A. Aziz, H. Shaikh, A. Abbas, K. E. Zehra, and B. Javed, “Microscopic Techniques for Nanomaterials Characterization: A Concise Review,” *Microsc Res Tech*, vol. 88, no. 5, pp. 1599–1614, May 2025, doi: 10.1002/JEMT.24799;CTYPE:STRING:JOURNAL.

[44] V. A. J. Jaques, E. Zikmundová, J. Holas, T. Zikmund, J. Kaiser, and K. Holcová, “Conductive cross-section preparation of non-conductive painting micro-samples for SEM analysis,” *Scientific Reports 2022 12:1*, vol. 12, no. 1, pp. 1–13, Nov. 2022, doi: 10.1038/s41598-022-21882-1.

[45] T. E. Davies, H. Li, S. Bessette, R. Gauvin, G. S. Patience, and N. F. Dummer, “Experimental methods in chemical engineering: Scanning electron microscopy and X-ray ultra-microscopy—SEM and XuM,” *Can J Chem Eng*, vol. 100, no. 11, pp. 3145–3159, Nov. 2022, doi: 10.1002/CJCE.24405.

[46] “Understanding the Difference between Magnification and Resolution in Scanning Electron Microscopy | Nanoscience Instruments.” Accessed: Nov. 11, 2025. [Online]. Available: https://www.nanoscience.com/blogs/understanding-the-difference-between-magnification-and-resolution-in-scanning-electron-microscopy/

[47] Y. Lin, M. Zhou, X. Tai, H. Li, X. Han, and J. Yu, “Analytical transmission electron microscopy for emerging advanced materials,” *Matter*, vol. 4, no. 7, pp. 2309–2339, Jul. 2021, doi: 10.1016/J.MATT.2021.05.005.

[48] L. Bijelić, F. Ruiz-Zepeda, and N. Hodnik, “The role of high-resolution transmission electron microscopy and aberration corrected scanning transmission electron microscopy in unraveling the structure–property relationships of Pt-based fuel cells electrocatalysts,” *Inorg Chem Front*, vol. 11, no. 2, pp. 323–341, Jan. 2024, doi: 10.1039/D3QI01998E.

[49] C. Ophus, “Quantitative Scanning Transmission Electron Microscopy for Materials Science: Imaging, Diffraction, Spectroscopy, and Tomography,” *Annu Rev Mater Res*, vol. 53, no. Volume 53, 2023, pp. 105–141, Jul. 2023, doi: 10.1146/ANNUREV-MATSCI-080921-092646/CITE/REFWORKS.

[50] Y. Lin, M. Zhou, X. Tai, H. Li, X. Han, and J. Yu, “Analytical transmission electron microscopy for emerging advanced materials,” *Matter*, vol. 4, no. 7, pp. 2309–2339, Jul. 2021, doi: 10.1016/J.MATT.2021.05.005.

[51] H. Ahmed *et al.*, “Recovery of oxidized two-dimensional MXenes through high frequency nanoscale electromechanical vibration,” *Nat Commun*, vol. 14, no. 1, pp. 1–9, Dec. 2023, doi: 10.1038/S41467-022-34699-3;SUBJMETA.

[52] J. Y. Kim *et al.*, “Proton-Coupled Electron Transfer on Cu2O/Ti3C2Tx MXene for Propane (C3H8) Synthesis from Electrochemical CO2 Reduction,” *Advanced Science*,

vol. 11, no. 39, p. 2405154, Oct. 2024, doi: 10.1002/ADVS.202405154;SUBPAGE:STRING:FULL.

[53] O. Cetin, O. Cakir, S. Koylan, D. Doganay, Y. Khan, and H. E. Unalan, "All-Solution Processed, Highly Stable MXene/Cu Nanowire Networks for Flexible Transparent Thin-Film Heaters," *ACS Appl Nano Mater*, vol. 6, no. 23, pp. 22446–22458, Dec. 2023, doi: 10.1021/ACSANM.3C05027.

[54] X. Wang, R. Wang, L. Shi, and J. Sun, "Kinetically controlled synthesis of Cu nanowires with tunable diameters and their applications in transparent electrodes," *J Mater Chem C Mater*, vol. 6, no. 5, pp. 1048–1056, Feb. 2018, doi: 10.1039/C7TC05038K.

[55] L. Dou *et al.*, "Solution-Processed Copper/Reduced-Graphene-Oxide Core/Shell Nanowire Transparent Conductors," *ACS Nano*, vol. 10, no. 2, pp. 2600–2606, Feb. 2016, doi: 10.1021/ACSNANO.5B07651.